Modeling Three-Dimensional Interference and SIR in Highly Directional mmWave Communications

Roman Kovalchukov[†], Andrey Samuylov[†], Dmitri Moltchanov[†], Aleksandr Ometov[†],
Sergey Andreev[†], Yevgeni Koucheryavy[†], and Konstantin Samouylov[‡⋆]
[†]Tampere University of Technology, Tampere, Finland
[‡]Peoples' Friendship University of Russia (RUDN University), Moscow, Russia
[⋆]Institute of Informatics Problems, Federal Research Center "Computer Science and Control"
of the Russian Academy of Sciences, Moscow, Russia

***Abstract*—Recently, new opportunities for utilizing extremely high frequencies have become instrumental in developing fifth-generation (5G) mobile technology. The use of highly directional antennas in millimeter-wave (mmWave) bands poses an important question of whether two-dimensional modeling suffices to capture the resulting system performance. Accounting for the effects of human body blockage by mmWave transmissions, in this work we compare the performance of the conventional two-dimensional and the proposed three-dimensional modeling. With our stochastic geometry based approach, we consider the aggregate interference and signal-to-interference ratio (SIR) to be the main metrics of interest. Both counterpart models attempt to capture the inherent behavior of 5G mmWave systems by incorporating the effects of human body blockage and antenna directivity. We thus deliver a realistic numerical assessment by comparing the three-dimensional modeling with its two-dimensional projection to reveal the resulting discrepancy.**

***Index Terms*—Interference, SIR, 3D modeling, mmWave, directional antennas, blockage, 5G**

I. Introduction

With adoption of advanced communication technology in the forthcoming 5G networks [1], the wireless community envisions that multiple handheld and wearable devices are to be placed on and around user bodies [2]. These capable devices may need to cooperate in proximity while utilizing the emerging millimeter-wave (mmWave) radios in ultra-dense scenarios to enable extremely high network capacity and achieve lower latency as compared to conventional communication under 6GHz [3]. As a result, mmWave systems are expected to soon become an integral part of the prospective 5G mobile networks by supporting unprecedented data rates at the air interface along with more efficient spatial frequency reuse.

To this end, the use of mmWave bands, such as 28GHz, 60GHz, and 72GHz, has recently been considered, which calls for the need of highly directional antennas. The utilization of 'pencil' beams significantly reduces the interfering signals and increases the performance under specific conditions. There is also an opportunity to approach operation in noise-limited regime [4]. Another feature of mmWave band is the incapability of transmissions to "travel around" the objects whose size is larger than several centimeters. Hence, in these systems, various objects in the channel, such as human bodies, lampposts, and buildings, act as blockers [5].

The evolution of communication systems in 5G era is accompanied by the increasing complexity of networking use cases. The envisioned utilization of drones to deliver service to crowds on the move as well as the use of "high-end" wearable electronics (e.g., augmented-reality glasses) will enable connectivity in three dimensions [6]. Similarly, new highly dense 5G scenarios, e.g., shopping mall deployments, meet another emerging paradigm named device-to-device (D2D) communication that is expected to further push (beyond-)5G wireless systems to explore the third dimension.

Today, stochastic geometry remains the most commonly applied tool for performance analysis of wireless systems. The performance of mmWave deployments has been extensively addressed in this context over the last several years. The moments of interference and signal-to-interference ratio (SIR) for mmWave systems in the presence of blockage have been derived in [7]. The Laplace transform (LT) of pdfs of interference and SIR in the absence of blockage have been obtained in [8]. The LT of SIR for mmWave system operating at 28GHz has been reported in [9], [10]. At the same time, despite the use of directional antennas and complex blockage situations, all of the referenced works assumed two-dimensional deployments. However, modeling in three dimensions may capture the actual performance more adequately for highly directional systems.

We here address the question of when two-dimensional models for mmWave systems are no longer able to accurately characterize user performance metrics, including the aggregate interference and SIR. This paper is continued with the system model in Section II. Further, in Section III, we analyze a three-dimensional deployment by taking into account the inherent properties of mmWave systems, including blockage effects on the line-of-sight (LoS) path and high directivity of the transmit antennas. Two-dimensional analysis is sketched in Section IV. In Section V, we provide numerical results and make conclusions. Our study is summarized in the last section.

II. System Model and Parameters

1) Considered Deployment Model: Our descriptive communication scenario in $\Re^3$ is demonstrated in Fig. 1, where green bars represent the communicating pair of interest, red bars are the interfering pair, and blue bars are the possibly interfering nodes that are currently in the state of blockage. Assume that the locations of receivers, labeled as X_{R_i}, $i = 1, 2, \ldots$, are modeled by a Poisson point process in $\Re^2$ with the intensity of λ. The receivers are located at height H_R that is assumed to follow an exponential distribution with the parameter μ.

Each receiver is associated with a transmitter labeled as X_{T_i}. Positions of the transmitters are distributed uniformly

$$E[P^n(r)] = \frac{A^n \mu \pi^{\frac{3}{2}} \left(\frac{r}{\mu}\right)^{\frac{1}{2}-\frac{n\gamma}{2}} \left[2J^{\mu r}_{n\gamma-1} \csc(n\pi\gamma) - J^{\mu r}_{\frac{1-n\gamma}{2}} \sec\left(\frac{n\pi\gamma}{2}\right) + \csc\left(\frac{n\pi\gamma}{2}\right) H^{\mu r}_{\frac{1-n\gamma}{2}}\right]}{2^{\frac{n\gamma}{2}+\frac{1}{2}}\Gamma\left(\frac{n\gamma}{2}\right)}. \quad (1)$$

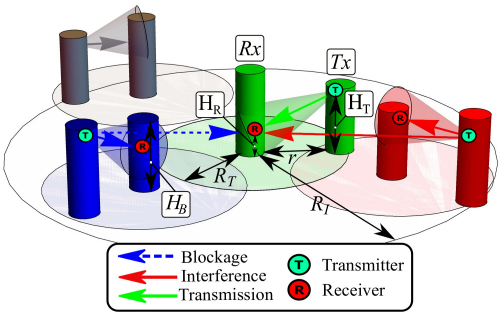

Fig. 1. Considered three-dimensional mmWave communication scenario.

within the circle of radius R_T centered at the receiver. The transmitters are assumed to utilize the same frequency channel, thus acting as interferers to the tagged receiver. Among the transmitter-receiver pairs, we randomly tag an arbitrary one. We limit the area around the tagged receiver to the radius R_I. The interference created by the transmitters located outside is assumed to be negligible, i.e., lower than the noise floor. R_I is computed as a function of the propagation model, transmit power, and antenna directivity. We also assume that all transmitters communicate continuously, so that all of the users can contribute to the interference.

The heights of transmitters and receivers, H_T and H_R, follow an exponential distribution with the parameter μ, i.e., the device could be located not only in the user's hand but anywhere on the body. Receivers and transmitters are associated with the communicating entities, e.g., humans represented by cylinders with the radius, r_B, while the height, H_B, follows an exponential distribution with the parameter μ_B, $\mu_B < \mu$.

2) Blockage Model: We assume that users may block the LoS path between the interferers and the tagged receiver. Note that the interferers themselves as well as other obstacles (e.g., those not involved into the communication process) may act as blockers. Therefore, in addition to the consideration of active communicating pairs with the density of λ, we also assume that the intensity of people not engaged into communication is λ_N. The overall intensity of blockers is $\lambda = \lambda_B + \lambda_N$.

3) Propagation and Antenna Models: The path loss model is $L_P(r) = Ar^{-\gamma}$ [11], where γ is the loss exponent, A is the factor accounting for the transmit power and antenna gains.

Following [12], [13], we assume the cone antenna radiation pattern model. In this work, we only consider the transmit antenna directivity, assuming that the receiver sensitivity is omnidirectional. The directivity of the transmit antenna is modeled as a conical zone with the angle of α, as shown in Fig. 2. This model is an abstraction assuming no side lobes and constant power at a certain distance from the transmitter.

The coefficient A corresponds to the directivity angle α and is estimated as follows. The surface area of a wavefront at distance r from the radiator is $S_A = 2\pi r^2[1 - \cos(\alpha/2)]$. Hence, the power density at the wavefront is given by

$$P_{Rx} = P_{Tx}/S_A = Ar^{-\gamma}P_{Tx}/4\pi, \quad (2)$$

where P_{Tx} refers to the transmit power, leading to $A = 2/[1-\cos(\alpha/2)]$.

4) Metrics of Interest: We compare the two- and three-dimensional models based on the first moment of interference and SIR. The aggregate interference and SIR are

$$I = A\sum_{i=1}^{N} d_i^{-\gamma},\ S = \frac{Ad_0^{-\gamma}}{A\sum_{i=1}^{N} d_i^{-\gamma}} = \frac{d_0^{-\gamma}}{\sum_{i=1}^{N} d_i^{-\gamma}}, \quad (3)$$

where N is a Poisson random variable (RV) with the mean $\lambda\pi R_I^2$, d_i, $i = 0, 1, \ldots, N$, are distances in $\Re^3$.

III. Three-Dimensional Model Analysis

A. Moments of Interference

Using the Campbell theorem, the first and the second moments of the aggregate interference at the receiver are [14]

$$E[I^n] = \int_{r_B}^{R_I} E[P^n(r)]\,(1 - p_B(r))\,p_C(r)2\lambda\pi r dr, \quad (5)$$

where $2\lambda\pi r dr$ is the probability of having the interferer in the infinitesimal increment of the circumference, $p_B(r)$ is the probability of the LoS blockage at distance r, $p_C(r)$ is the probability that the transmit and receive antennas of an interfering pair are oriented in such a way that the interferer contributes to the aggregate interference at the tagged receiver, $E[P^n(r)]$, $n = 1, 2$ are the first and the second moments of the interfering signal, conditioned on the distance between the receiver and the interferer, r. The only unknowns are $E[P^n(r)]$, $p_B(r)$, and $p_C(r)$.

B. Conditional Moments of Interfering Signal, $E[P^n(r)]$

Consider $E[P^n(r)]$, $n = 1, 2, \ldots$, that is, raw moments of the interfering signal power conditioned on the distance r. The power of the interfering signal is written as

$$P(r) = A\left(\sqrt{(H_T - H_R)^2 + r^2}\right)^{-\gamma}, \quad (6)$$

where $\sqrt{(H_T - H_R)^2 + r^2}$ is the path traveled by a signal, r is a parameter, while H_T and H_R are the only RVs involved.

Due to the exponential nature of H_T and H_R, the modulo of the difference $|H_T - H_R|$ follows the exponential distribution with the same parameter μ. Recalling that we are only

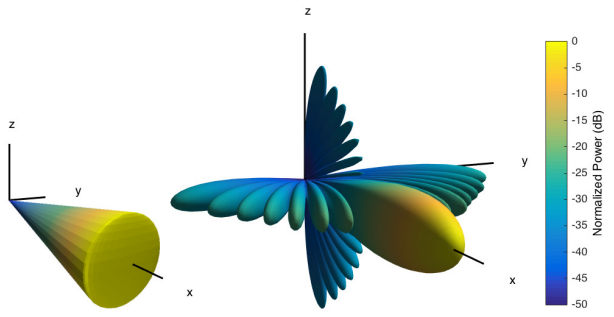

Fig. 2. Assumed vs. real antenna radiation pattern.

$$f_{\eta_1,\eta_4}(y_1,y_4)=\iiint\limits_{\mathrm{R}^3} f_{\xi_1^n}\left[\varphi_i(y_1^n))\right]|J|\,dy_2dy_3dy_5=\int\limits_0^{R_I}\int\limits_0^{R_T}\int\limits_{l(y_i)}^{\infty}\frac{4\mu^3y_3^2y_5^2\mathrm{e}^{-\mu(y_3\tan(y_1)+3y_2+y_5\tan(y_4))}}{\sec^{-2}(y_1)\sec^{-2}(y_4)R_I^2R_T^2}dy_2dy_3dy_5=$$

$$=\int\limits_0^{R_I}\int\limits_0^{R_T}\frac{4\mu^2y_3^2y_5^2e^{-\mu(3l(y_i)+y_3\tan(y_1)+y_5\tan(y_4))}}{\sec^{-2}(y_1)\sec^{-2}(y_4)3R_I^2R_T^2}dy_3dy_5=\int\limits_0^{R_I}f_{\eta_1\eta_4\eta_5}(y_1,y_4,y_5)dy_5. \quad (4)$$

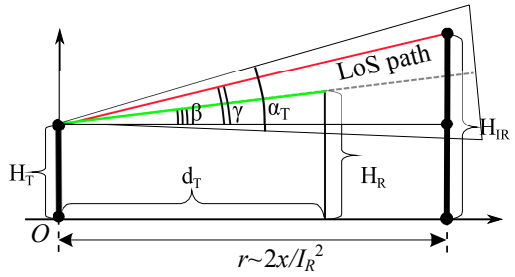

Fig. 3. An illustration of interference in three dimensions.

interested in the moments of $P(r)$, the distribution of $P(r)$ is not required. The moments of $P(r)$ are thus [15]

$$E[P^n(r)]=\int_0^{\infty}\mu e^{-\mu y}A^n\left(\sqrt{y^2+r^2}\right)^{-n\gamma}dy. \quad (7)$$

The moments of the interfering signal are provided in (1), where $\Gamma(z)$ is the Euler Gamma function, J_n^z is the Bessel function of the first kind, and H_n^z is the Struve function.

C. Directional "Hitting" Probability

The probability $p_C(r)$ can be approximated by

$$p_C(r)=p_V(r)p_H(r), \quad (8)$$

where $p_H(r)$ is the probability that the interferer "hits" the tagged receiver in two dimensions, $p_V(r)$ is the probability that such "hitting" also occurs in the third dimension.

The two-dimensional "hitting" probability, p_H, is given by

$$p_H(r)=\alpha r/2\pi r=\alpha/2\pi. \quad (9)$$

Considering $p_V(r)$ in Fig. 3, we observe that it corresponds to the probability $|\beta-\theta|<\alpha/2$, where β and θ are the transmit angles of the tagged transmitter and the interferer, respectively. Note that β and θ are dependent, as they share the same RV, H_R. The sought probability can be written as

$$p_V(r)=\int_{-\frac{\pi}{2}}^{\frac{\pi}{2}}\int_{y_4-\frac{\alpha}{2}}^{y_4+\frac{\alpha}{2}}f_{\beta,\theta}(y_1,y_4)dy_1dy_4, \quad (10)$$

where $f_{\beta,\theta}(y_1,y_4)$ is the joint probability density function (jpdf) of β and θ.

Let $\xi^n=\{\xi_1,\ldots,\xi_4\}=\{H_R,H_T,d_T,H_I\}$ and observe that its jpdf has the multiplicative form due to independence of the involved components, i.e.,

$$f_{\xi^n}(r^n)=\mu e^{-\mu x_1}\mu e^{-\mu x_2}(2x_3/R_T^2)\mu e^{-\mu x_4}. \quad (11)$$

Let also $\eta^m=\{\eta_1,\eta_4\}=\{\beta,\theta\}$. Since the number of target RVs, m, is lower than the number of input RVs, n, we complement the set of target RVs with auxiliary ones as

$$\eta^n=\{\eta_1,\ldots,\eta_4\}=\{\beta,H_T,d_T,\theta\}. \quad (12)$$

Hence, the transformation is

$$\begin{cases}y_1=f_1(x^n)=\beta=\arctan[(x_1-x_2)/x_3],\\ y_4=f_4(x^n)=\theta=\arctan[(x_4-x_2)/r],\end{cases} \quad (13)$$

and auxiliary functions are $f_i(x^n)=x_i$, $i=\{2,3\}$.

The inverses are bijections in the domains of interest, i.e.,

$$\begin{cases}x_1=\phi_1(y^n)=y_2+y_3\tan y_1,\\ x_4=\phi_4(y^n)=y_2+r\tan y_4,\end{cases} \quad (14)$$

complemented with $x_i=\phi_i(y^n)=y_i$, $i=\{2,3\}$.

The jpdf is then represented as

$$f_{\eta^n}(y^n)=f_{\xi^n}\left[\phi_1(y^n),\ldots,\phi_n(y^n)\right]|\mathbb{J}|, \quad (16)$$

where the Jacobian of the transformation is $\mathbb{J}=y_3r\sec^2y_1\sec^2y_4$, and $f_{\xi^n}\left[\phi_1(y^n),\ldots,\phi_n(y^n)\right]$ is

$$f_{\xi^n}=\frac{2\mathrm{e}^{-y_2\mu-\mu(y_2+y_3\tan(y_1))-\mu(y_2+r\tan(y_4))}}{RT^2}. \quad (17)$$

Denoting $l(y_i)=\max(0,-y_3\tan y_1,-r\tan y_4)$, we obtain (4). Performing the last integration, we calculate the jpdf of β and θ, $f_{\beta,\theta}(y_1,y_4)$ as in (15).

The integration according to (10) does not lead to a closed-form solution due to the complex form of the final integrand. Furthermore, even the numerical integration is time-consuming. However, the probability $p_V(r)$ can still be obtained in a simple form as a sum of the closed-form terms and simple integrals. To alleviate the integration problems, we first obtain the probability of the complementary event, $\{|\beta-\theta|>\alpha/2\}$, and then perform the last integration in (4). Separating the jpdf of angles β and θ in (4) into the set of subregions demonstrated in Fig. 4, and integrating over the region where $|\beta-\theta|>\alpha/2$, we represent $p_V(r)$ as

$$p_V(r)=1-\sum_{i=1}^{12}\int\int_{\Omega_i}f_{\beta,\theta}(y_1,y_4)dy_1dy_4. \quad (18)$$

As Fig. 4 indicates, the integrands in (18) take two principal forms. Those corresponding to regions $1-8$ can be obtained easily. As an example, by considering region 2 we have

$$I_2=\iint_{\Omega_2}f_{\beta,\theta}(y_1,y_4)dy_1dy_4=$$

$$=\int\limits_{\frac{\alpha}{2}}^{\frac{\pi}{2}}\int\limits_{-\frac{\pi}{2}}^{0}\frac{r\csc(y_1)\sec(y_1)\sec^2(y_4)}{6R_T^2\mu e^{r\mu\tan(y_4)}}[2e^{2R_T\mu\tan(y_1)}R_T^2\mu^2+$$

$$+\frac{\cot^2(y_1)}{e^{-2R_T\mu\tan(y_1)}}-\frac{2R_T\mu\cot(y_1)}{e^{-2R_T\mu\tan(y_1)}}-\cot^2(y_1)]dy_1dy_2=$$

$$=\int_{\frac{\alpha}{2}}^{\frac{\pi}{2}}\frac{e^{-r\mu\tan(y4)}r\mu\sec(y_4^2)}{6}dy_2=\frac{e^{-r\mu\tan(\alpha/2)}}{6}. \quad (19)$$

$$f_{\beta,\theta}(y_1,y_4)=\begin{cases}\frac{-4r\cot(y_1)\csc^2(y_1)\sec^2(y_4)[1-e^{R_T\mu\tan(y_1)}+2R_T\mu\tan(y_1)+RT^2\mu^2\tan^2(y_1)]}{3R_T^2\mu e^{\mu[R_T\tan(y_1)+r\tan[y_4]]}}, & y_1\geq 0\cap y_4\geq 0,\\ \frac{4r\cot(y_1)\csc^2(y_1)\sec^2(y_4)[e^{R_T\mu\tan(y_1)}-2R_T\mu\tan(y_1)-R_T^2\mu^2\tan^2(y_1)-1]}{3RT^2\mu e^{R_T\mu\tan(y_1)+2r\mu\tan(y_4)}}, & y_1\geq 0\cap y_4<0,\\ & y_4<0\cap\tan y_1\geq\tan y_4,\\ \frac{2e^{2R_T\mu\tan(y_1)}RT^2\mu^2-2e^{2R_T\mu\tan(y_1)}R_T\mu\cot(y_1)-\cot^2(y_1)+e^{2R_T\mu\tan(y_1)}\cot^2(y_1)}{6r^{-1}\csc^{-1}(y_1)\sec^{-1}(y_1)\sec^{-12}(y_4)R_T^2\mu e^{r\mu\tan(y_4)}}, & y_1<0\cap y_4\geq 0,\\ \frac{r\cot(y_1)\csc(y_1)\sec^2(y_4)}{6R_T^2\mu e^{r\mu\tan(y_4)}}\times & \\ \Big(e^{2R_T\mu\tan(y_1)}\csc(y_1)-9e^{2r\mu\tan(y_4)}\csc(y_1)+8e^{3r\mu\tan(y_4)}\csc(y_1)- & \\ -2e^{2R_T\mu\tan(y_1)}R_T\mu\sec(y_1)+2e^{2R_T\mu\tan(y_1)}R_T^2\mu^2\sec(y_1)\tan(y_1)-, & \text{elsewhere.}\\ -6e^{2r\mu\tan(y_4)}r\mu\csc(y_1)\tan(y_4)-6e^{2r\mu\tan(y_4)}r^2\mu^2\csc(y_1)\tan^2(y_4)\Big), & \end{cases}\tag{15}$$

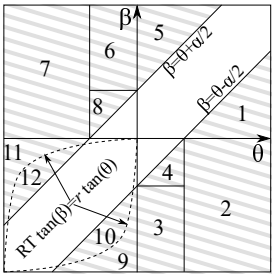

Fig. 4. Regions of integration for (18).

More complex integrals corresponding to regions $9-12$ can be reduced to single integrals that can further be evaluated numerically. Using region 9 as an example, we have

$$I_9=\iint_{\Omega_9} f_{\beta,\theta}(y_1,y_4)dy_1dy_4= \tag{20}$$

$$=\int_{\frac{\alpha}{2}}^{\frac{\pi}{2}}\int_{\frac{-\pi}{2}}^{m(y_4)}\frac{2r[R_T\mu\cot(y_1)-e^{R_T\mu\tan(y_1)}\csc^2(y_1)]}{3\sec^{-2}(y_4)R_T^2\mu e^{R_T\mu\tan(y_1)-2r\mu\tan(y_4)}}=$$

$$=\int_{\frac{-\pi}{2}}^{\frac{-\alpha}{2}}\frac{2r\sec^2(y_4)e^{2r\mu\tan(y_4)}}{3R_T^2\mu}\Big(-1-\frac{R_T^2\mu^2}{2}+$$

$$+e^{-R_T\mu\tan[m_2(y_4)]}\Big[1-R_T\mu\cot[m_2(y_4)]+$$

$$+\Big(e^{R_T\mu\tan[m_2(y_4)]}-1\Big)\csc^2[m_2(y_4)]\Big]\Big)dy_4, \tag{21}$$

where

$$m_1(y_4)=\min\left(y_4-\alpha/2,\arctan[r\tan(y_4)/R_T]\right),$$
$$m_2(y_4)=\max\left(y_4+\alpha/2,\arctan[r\tan(y_4)/R_T]\right). \tag{22}$$

D. Blockage Probability

The derivation of the blockage probability $p_B(r)$ is illustrated in Fig. 5 (a). Let G_r, $0<r<R_I$, be the RV denoting the height of the LoS path at x-coordinate uniformly distributed in $(0,R_I)$. We thus have

$$G_r=(H_R-H_T)Y/r+H_T-H_B, \tag{23}$$

where Y is the RV uniformly distributed in $(0,r)$.

The probability that a single blocker located at the distance r from the receiver occludes the LoS path is given by

$$p_{B,1}(r)=1-Pr\left\{(H_R-H_T)Y/r+H_T-H_B>0\right\}. \tag{24}$$

Knowing $p_{B,1}(r)$ and applying the properties of the Poisson process, we establish the overall blockage probability as

$$p_B(r)=1-\sum_{i=0}^{\infty}\frac{(2\lambda r_B r)^i}{i!e^{2\lambda r_B r}}[1-p_{B,1}(r)]^i=$$

$$=1-e^{-2\lambda r_B r}-\sum_{i=1}^{\infty}\frac{(2\lambda r_B r)^i}{i!e^{2\lambda r_B r}}[1-p_{B,1}(r)]^i, \tag{26}$$

where $p_{B,1}(r)=Pr\{G_r-H_B>0\}$ is the unknown term.

Let $\xi^n=\{\xi_1,\xi_2,\xi_3,\xi_4\}=\{H_B,H_R,H_T,Y\}$ with jpdf

$$f_{\xi^n}(x^n)=\frac{\mu_B e^{-\mu_B x_1}\mu e^{-\mu x_2}\mu e^{-\mu 4x_3}}{r}, \tag{27}$$

and define $\{\eta_1\}=\{G_r\}$ as the target variable.

Supplementing with auxiliary variables

$$\eta^n=\{\eta_1,\eta_2,\eta_3,\eta_4\}=\{G_r,H_R,H_T,Y\}, \tag{28}$$

the transformation at hand reads as

$$y_1=f(x^n)=G_r=(x_2-x_3)x_4/A+x_3-x_1,$$

where the auxiliary functions are $f_i(x^n)=x_i$, $i\in\{2,3,4\}$.

The inverse transformation is a bijection

$$x_1=\varphi_1\left(y_1^n\right)=-(Ay_1-Ay_3-y_2y_4+y_3y_4)/A,$$

complemented with $x_i=\phi_i(y^n)=y_i$, $i\in\{2,3,4\}$.

The jpdf can then be represented as

$$f_{\eta^n}(y^n)=f_{\xi^n}[\phi_1(y^n),\ldots,\phi_n(y^n)]|\mathbb{J}|, \tag{29}$$

where $f_{\xi^n}[\phi_1(y^n),\ldots,\phi_n(y^n)]$ is given by

$$f_{\xi_1^n}\left[\varphi_i\left(y_1^n\right)\right]=\frac{\mu^2\mu_B}{A}e^{\frac{\mu_B(Ay_1-Ay_3-y_2y_4+y_3y_4)}{A}-y_2\mu-y_3\mu}, \tag{30}$$

and the Jacobian is $\mathbb{J}=\partial\varphi_1\left(y^n\right)/\partial y_1=-1$.

The pdf of G_r can now be written as (25), where

$$l_1(i_i)=\max\left\{0,\frac{y_2y_3-Ay_2}{y_3},\frac{-Ay_2+Ay_4+y_2y_3}{y_3}\right\}, \tag{31}$$

and the final integrand takes the following form

$$f_{\eta_1\eta_4}(y_1,y_4)=\frac{(A-2y_4)^{-1}\mu\mu_B e^{-\frac{A\mu y_1}{A-y_4}-\frac{A\mu y_1}{y_4}}}{(A\mu+A\mu_B-\mu_B y_4)(A\mu+\mu_B y_4)}=$$

$$=\Big(A^2\mu e^{\frac{A\mu y_1}{y_4}}-\mu_B y_4^2 e^{\frac{A\mu y_1(A-2y_4)}{y_4(A-y_4)}+\frac{A\mu y_1}{A-y_4}}+$$

$$-A\mu_B y_4 e^{\frac{A\mu y_1}{A-y_4}}-A\mu y_4 e^{\frac{A\mu y_1}{A-y_4}}-2A\mu y_4 e^{\frac{A\mu y_1}{y_4}}+$$

$$+A\mu y_4 e^{\frac{A\mu y_1(A-2y_4)}{y_4(A-y_4)}+\frac{A\mu y_1}{A-y_4}}+\mu_B y_4^2 e^{\frac{A\mu y_1}{A-y_4}}+$$

$$+A\mu_B y_4 e^{\frac{A\mu y_1(A-2y_4)}{y_4(A-y_4)}+\frac{A\mu y_1}{A-y_4}}\Big). \tag{32}$$

$$f_{\eta_1}(y_1)=\iiint\limits_{\mathrm{R}^3} f_{\xi_1^n}[\varphi_i(y_1^n)]|J|dy_2dy_3dy_4=\int\limits_0^A\int\limits_0^\infty\int\limits_{l_1(y_i)}^\infty \frac{\mu^2\mu_B}{A}e^{\frac{\mu_B(Ay_1-Ay_3-y_2y_4+y_3y_4)}{A}-y_2\mu-y_3\mu}dy_2dy_3dy_4=$$

$$=\int\limits_0^A\int\limits_0^\infty \frac{\mu^2\mu_B}{A\mu+\mu_By_4}e^{\frac{A\mu_By_1-Ay_3(\mu+\mu_B)+\mu_By_3y_4-(A\mu+\mu_By_4)\max\left\{0,A(y_1-y_3)y_4^{-1}+y_3\right\}}{A}}dy_3dy_4=\int\limits_0^A f_{\eta_1\eta_4}(y_1,y_4)dy_4. \quad (25)$$

The integral in (26) cannot be evaluated in the closed-form. However, changing the order of integration, we arrive at

$$p_{B,1}(r)=\int\limits_0^A\int\limits_0^\infty f_{\eta_1\eta_4}(y_1,y_4)dy_1dy_4=\frac{2\mu^2\log\left(\frac{\mu}{\mu+\mu_B}\right)}{\mu_B\left(2\mu+\mu_B\right)}. \quad (33)$$

Substituting the latter result into (26) and integrating, we produce the following closed-form expression for $p_B(r)$

$$p_B(r)=1-\left(\frac{\mu}{\mu+\mu_B}\right)^{\frac{4r_Br\lambda\mu^2}{2\mu\mu_B+\mu_B^2}}. \quad (34)$$

E. SIR Analysis

To derive the mean SIR, we use the Taylor series expansion of the SIR function, $S=g(x,y)=P(x)/I(y)$. The second-order approximation is obtained by expanding $g(x,y)$ around $\vec{\mu}=(E[P],E[I])=(\mu_P,\mu_I)$. Simplifying, we obtain

$$E[g(\vec{\mu})]\approx g(\vec{\mu})+\frac{g''_{xx}(\vec{\mu})\sigma_P^2+2g''_{xy}K_{P,I}+g''_{yy}(\vec{\mu})\sigma_I^2}{2}, \quad (35)$$

where $K_{P,I}$ is the covariance between P and I, while σ_J^2 and σ_I^2 are the variances of P and I, respectively.

Observing that

$$g''_{xx}(x,y)=0,\ g''_{x,y}(x,y)=-y^{-2},\ g''_{yy}(x,y)=2x/y^2, \quad (36)$$

we arrive at the following approximation

$$E[P/I]\approx\mu_P/\mu_I-K_{P,I}/\mu_I^2+\sigma_I^2\mu_P/\mu_I^3. \quad (37)$$

To obtain the mean SIR according to (37), the following is required: (i) mean received signal strength, (ii) first two moments of the aggregate interference, and (iii) covariance between P and I. The mean received signal strength is obtained similarly to (6) by observing that r is also a RV with pdf $f_r(x)=2x/R_T^2$ and is given by (38), where Γ_a^z is the incomplete Gamma function. The first two moments of the aggregate interference are provided in (5).

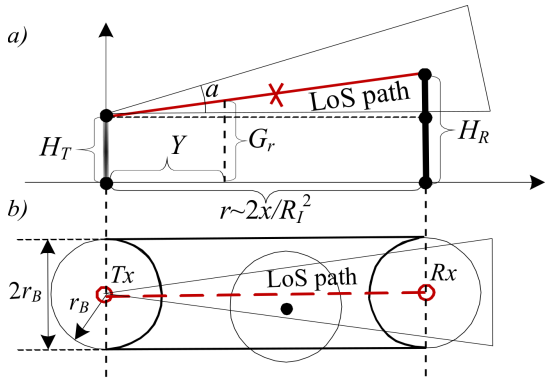

Fig. 5. An illustration of human body blockage in three dimensions.

Representing the covariance as $K_{P,I}=E[PI]-\mu_P\mu_I$, we write the first mixed moment as

$$E[PI]=E\Big[AX_0^{-\gamma}\sum_{i=1}^N AX_i^{-\gamma}\Big], \quad (39)$$

where X_0 is the distance between the transmitter and the receiver, X_i, $i=1,2,\ldots,N$, are the distances between the interferers and the receiver, and N is the number of interferers.

Applying the Wald's identity [15], we obtain

$$E[PI]=A^2\lambda\pi R_I^2p_Cp_BE[(X_iX_0)^{-\gamma}], \quad (40)$$

where $E[N]=\lambda\pi R_I^2p_Bp_C$ and

$$p_B=\int_{r_B}^{R_I}p_B(r)dr,\ p_C=\int_{r_B}^{R_I}p_C(r)dr. \quad (41)$$

Rewriting $E[(X_0X_i)^{-\gamma}]$ as

$$E[([(H_R-H_T)^2-r_0][(H_R-H_I)^2-r_i])^{-\frac{\gamma}{2}}], \quad (42)$$

where r_0 is a constant, we see that $E[(X_0X_i)^{-\gamma}]$ is given by

$$\int\limits_0^{R_I}\int\limits_0^{R_T}\int\limits_0^\infty\int\limits_0^\infty\int\limits_0^\infty\frac{[(x_1-x_2)^2+x_5^2]^{-\frac{\gamma}{2}}}{[(x_1-x_3)^2+x_4^2]^{\frac{\gamma}{2}}}f(x_1,..,x_5)dx_1..dx_5, \quad (43)$$

where jpdf is given by

$$f(x_1,x_2,x_3,x_4)=\mu^3e^{-\mu(x_1+x_2+x_3)}4x_4x_5/(R_TR_I)^2. \quad (44)$$

Note that (43) cannot be obtained in the closed-form. Furthermore, the procedure in question highly depends on the order of integration. Choosing it as indicated above (43), can reduce it to the sum of single integrals that may be obtained numerically.

IV. Two-Dimensional Model

Below, we follow [12], [13] to sketch the analysis for the two-dimensional model. The key difference between the two- and the three-dimensional models is in the probability of blockage, $p_B(r)$, and the directional "hitting" probability, $p_C(r)$. For the two-dimensional model, $p_C(r)$ reduces to $p_C(r)=p_H(r)=\alpha/2\pi$ in (9).

The blockage probability in the two-dimensional case can be approximated by the probability that the center of at least one blocker falls into the LoS blockage zone, with the sides $2r_B$ and X, where X is the RV with pdf $f_X(x)=2x/R_T^2$. The conditional blockage probability is given by the void probability of the spatial Poisson process, see, e.g., [5],

$$p_B(r)=e^{-2\lambda r_Br}. \quad (45)$$

$$E[P]=\frac{8\mu^{\frac{\gamma n}{2}}\csc(\pi\gamma n)R_T^{\frac{\gamma n}{2}}-\mu^{\frac{3}{2}}R_T^{\frac{3}{2}}2^{\frac{\gamma n+1}{2}}\Gamma\left(\frac{n\gamma-1}{2}\right)\left(2\csc(\pi\gamma n)J^{R_T\mu}_{\frac{n\gamma-3}{2}}+\sec\left(\frac{\pi\gamma n}{2}\right)J^{R_T\mu}_{\frac{3-n\gamma}{2}}-\csc\left(\frac{\pi\gamma n}{2}\right)H^{R_T\mu}_{\frac{3-n\gamma}{2}}\right)}{4\Gamma(n\gamma-1)\pi^{-1}A^{-n}\mu^{2-\frac{\gamma n}{2}}R_T^{\frac{\gamma n}{2}+2}}. \quad (38)$$

Using (5), the moments of interference are

$$E[I^n]=\int_{r_B}^{R_I}(Ar^{-\gamma})^n(1-e^{-2\lambda r_B r})\frac{\alpha}{2\pi}2\lambda\pi r dr= \\ =A^n\alpha\lambda\Big[\frac{E_{n\gamma-1}\left(-2\lambda r_B^2\right)}{r_B^{\gamma n-2}}-\frac{E_{n\gamma-1}\left(-2\lambda r_B R_I\right)}{R_I^{\gamma n-2}}\Big], \quad (46)$$

where $E_n(x)$ is the exponential integral function [16].

Then, the mean can be estimated by using (37), where $K_{P,I}=0$ for the two-dimensional model, while the moments of interference are provided in (46) and the mean received signal is given by

$$E[P]=\int_{r_B}^{R_T}Ax^{-\gamma}\frac{2x}{R_T^2}dx=\frac{2A\left(r_B^{2-\gamma}-R_T^{2-\gamma}\right)}{(\gamma-2)R_T^2}. \quad (47)$$

V. Numerical Analysis

In the two-dimensional deployment, the results for the moments of interference and the SIR moments are available in a simple form, which only features the exponential integral functions that can be computed efficiently with any given accuracy. Moving to three dimensions by considering the heights of entities, simple expressions are no longer available. The natural question is then "can we still apply two-dimensional models to accurately capture performance metrics?" The answer to this key question depends on the discrepancy that we allow and it may thus vary depending on the required accuracy. Below, we perform a numerical study of the error that arises as a result of replacing the three-dimensional model with its two-dimensional projection.

In our example D2D scenario the heights are chosen as $E[H_T]=E[H_R]=1.5$m and $E[H_B]=1.7$m. The radius of a blocker is $r_B=0.3$m. No additional field of blockers is assumed, i.e., only the communicating entities themselves produce blockage. The maximum distance of communication, R_T, is set to 3m. To facilitate comparison, we chose $A=1$. The radius of interference, R_I, is computed such that the interference from a user outside is lower than the noise floor, -174dBm. The antenna directivity, α, and the intensity of communicating pairs, λ, vary.

The accuracy of the considered two-dimensional model has been assessed in [12]. The comparison between the two models in terms of the mean interference as a function of λ is summarized in Fig. 6. The key difference between the two- and the three-dimensional models is in the presence of vertical "hitting" probability, p_V. Disregarding the latter by setting $p_V=1$, the three-dimensional model becomes closer to its two-dimensional counterpart. There still remains difference attributed to the effect of the three-dimensional blockage.

Further, Fig. 7 reports on the mean interference in dBm as a function of the antenna directivity, α, and the intensity of communicating pairs, λ. Our most important observation is the dramatic difference between the two- and the three-dimensional model. It is also important to note that the models demonstrate fundamentally different behavior as a function of λ. Particularly, the mean interference in the two-dimensional model grows as λ becomes smaller, while the opposite effect is observed in three dimensions showing that the difference between the models is not only quantitative but also qualitative.

The effect of antenna directivity, α, on the mean interference is as expected. Specifically, the gap between the models becomes higher as α decreases, thus highlighting the importance of utilizing three-dimensional models in the emerging communication systems. Both models converge as α approaches 2π. The increase in interference with the decrease of α is explained by the fact that with lower α the amount of energy reaching the tagged receiver grows. For larger values of α, this effect cannot be compensated by the decreased "hitting" probability. Since the "hitting" probability drops at a much faster rate as compared to the growth in the interference energy, there is a point after which the mean interference lowers.

The interference does not provide full information on the channel quality. Therefore, Fig. 8 quantifies the mean SIR for both models. As one may observe, the trends in the mean interference translate into the mean SIR. Specifically, there is a large gap between the models, which can reach tens of dBs for some values of (α,λ), where the two-dimensional model underestimates the actual SIR.

VI. Conclusions

In this paper, we proposed the use of three-dimensional modeling for performance assessment in the emerging mmWave systems, which takes into account the blockage effects as well as the directivity of the transmit antennas. Our formulated model is an extension of the conventional two-dimensional approach, which facilitates direct comparison between them. The resulting expressions for the mean interference and SIR are naturally more cumbersome and involve a series of integrals that cannot be solved in the closed-form or expressed in terms of the tabulated functions. Extending the model to the case of two-way antenna directivity further complicates the resulting expressions.

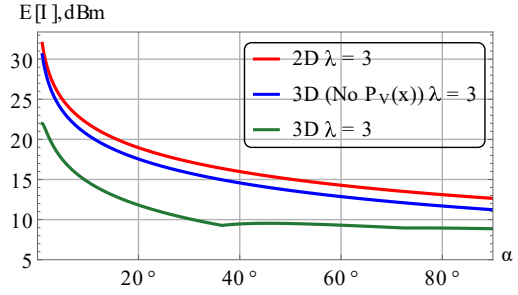

Fig. 6. Comparison of two- and three-dimensional models.

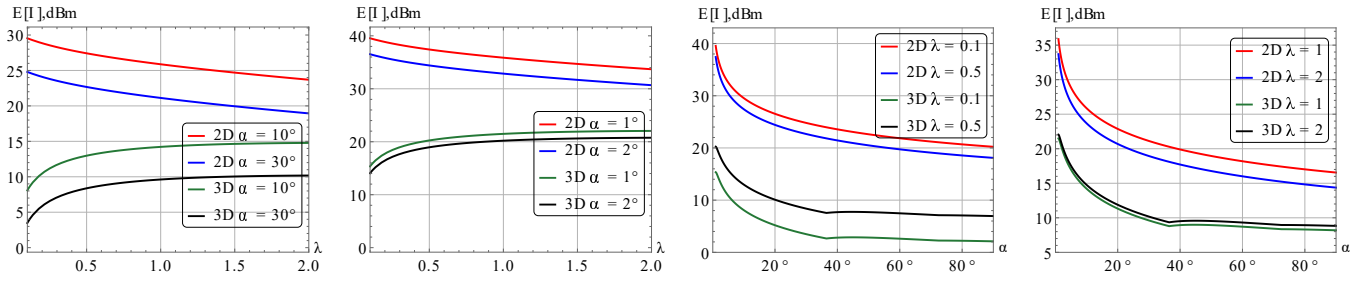

(a) Varying λ (b) Varying λ (c) Varying α (d) Varying α

Fig. 7. Comparing interference in two- and three-dimensional models: $E[H_T] = E[H_R] = 1.5$m, $E[H_B] = 1.7$m, $r_B = 0.3$, $R_T = 3$m, $A = 1$.

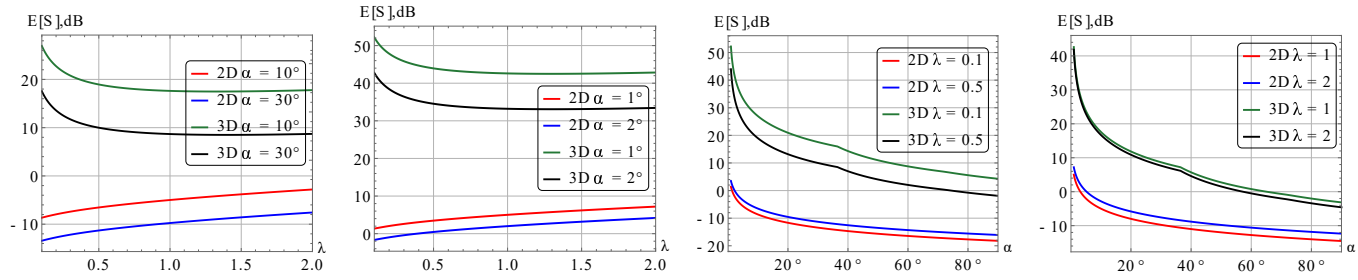

(a) Varying λ (b) Varying λ (c) Varying α (d) Varying α

Fig. 8. Comparing SIR in two- and three-dimensional models: $E[H_T] = E[H_R] = 1.5$m, $E[H_B] = 1.7$m, $r_B = 0.3$, $R_T = 3$m, $A = 1$.

Employing the proposed methodology, we demonstrated that the difference between the two- and the three-dimensional models can be extremely high already for our representative D2D scenario, where the variation in the mean heights of transmitters and blockers is insignificant for all realistic ranges of communicating pairs and antenna directivities. In our further studies, we plan to extend the present results to the two-way antenna directivity while reporting our findings for other practical 5G network deployments.

Acknowledgment

This work is supported by the WiFiUS project funded in part by the Academy of Finland. It is also supported by the "RUDN University Program 5-100" and funded by RFBR according to the research projects No. 16-07-00766 and No. 17-07-00845.

References

[1] Cisco, "Global mobile data traffic forecast 2016–2021." White Paper, 2017.

[2] G. George and A. Lozano, "Impact of reflections in enclosed mmWave wearable networks," in *Proc. of 6th International Workshop on Computational Advances in Multi-Sensor Adaptive Processing (CAMSAP)*, pp. 201–204, IEEE, 2015.

[3] K. Venugopal and R. W. Heath, "Location based performance model for indoor mmWave wearable communication," in *Proc. of International Conference on Communications (ICC)*, pp. 1–6, IEEE, 2016.

[4] J. G. Andrews, S. Buzzi, W. Choi, S. V. Hanly, A. Lozano, A. C. Soong, and J. C. Zhang, "What will 5G be?," *IEEE Journal on Selected Areas in Communications*, vol. 32, no. 6, pp. 1065–1082, 2014.

[5] M. Gapeyenko, A. Samuylov, M. Gerasimenko, D. Moltchanov, S. Singh, E. Aryafar, S.-p. Yeh, N. Himayat, S. Andreev, and Y. Koucheryavy, "Analysis of human-body blockage in urban millimeter-wave cellular communications," in *Proc. of International Conference on Communications (ICC)*, pp. 1–7, IEEE, 2016.

[6] A. Orsino, A. Ometov, G. Fodor, D. Moltchanov, L. Militano, S. Andreev, O. N. Yilmaz, T. Tirronen, J. Torsner, G. Araniti, *et al.*, "Effects of heterogeneous mobility on D2D-and drone-assisted mission-critical MTC in 5G," *IEEE Communications Magazine*, vol. 55, no. 2, pp. 79–87, 2017.

[7] V. Petrov, D. Moltchanov, and Y. Koucheryavy, "On the efficiency of spatial channel reuse in ultra-dense THz networks," in *In Proc. IEEE Globecom*, Dec. 2015.

[8] M. Di Renzo, "Stochastic geometry modeling and analysis of multi-tier millimeter wave cellular networks," *IEEE Transactions on Wireless Communications*, vol. 14, no. 9, pp. 5038–5057, 2015.

[9] K. Venugopal and R. Heath, "Millimeter Wave Networked Wearables in Dense Indoor Environments," *IEEE Access*, vol. 4, pp. 1205–1221, Apr. 2016.

[10] S. Singh, M. N. Kulkarni, A. Ghosh, and J. G. Andrews, "Tractable model for rate in self-backhauled millimeter wave cellular networks," *IEEE Journal on Selected Areas in Communications*, vol. 33, no. 10, pp. 2196–2211, 2015.

[11] S. Singh, R. Mudumbai, and U. Madhow, "Interference Analysis for Highly Directional 60-GHz Mesh Networks: The Case for Rethinking Medium Access Control," *IEEE/ACM Transactions on Networking*, vol. 19, pp. 1513–1527, Oct 2011.

[12] V. Petrov, M. Komarov, D. Moltchanov, J. M. Jornet, and Y. Koucheryavy, "Interference and SINR in Millimeter Wave and Terahertz Communication Systems With Blocking and Directional Antennas," *IEEE Transactions on Wireless Communications*, vol. 16, no. 3, pp. 1791–1808, 2017.

[13] V. Petrov, M. Komarov, D. Moltchanov, J. Jornet, and Y. Koucheryavy, "Interference Analysis of EHF/THF Communications Systems with Blocking and Directional Antennas," in *Proc. of Global Communications Conference (GLOBECOM)*, pp. 1–7, 2016.

[14] S. Chiu, D. Stoyan, W. Kendall, and J. Mecke, *Stochastic geometry and its applications*. Wiley, 2013.

[15] S. Ross, *Introduction to probability models*. Academic Press, 2010.

[16] M. Abramowitz and I. Stegun, *Handbook of Mathematical Functions with Formulas, Graphs, and Mathematical Tables*. Dover, 1965.